Bull. Mater. Sci. (2022)45:16
https://doi.org/10.1007/s12034-021-02601-4

© Indian Academy of Sciences

Density functional theory study of electronic and optical properties of ScN nitride in NaCl-B1, CsCl-B2, ZB-B3 and NiAs-B8 phases

BHILA OLIVER MNISI
Department of Physics, University of South Africa, Johannesburg 1709, South Africa
*For correspondence (bhila.oliver00@gmail.com)

MS received 13 November 2020; accepted 22 September 2021

Abstract. The structural, mechanical, electronic and optical properties of ScN nitride in NaCl-B1, CsCl-B2, zinc-blende (ZB)-B3 and NiAs-B8 phases were investigated by first-principle density functional theory. Mechanical properties are investigated, and the ScN in NaCl-B1, ZB-B3 and NiAs-B8 phases are mechanical stable indicating possible experimental synthesis except for CsCl. We note that NaCl-B1 possesses the highest hardness of 24.8 GPa. Band structures and density of states analysis indicate that NaCl-B1, ZB-B3 and NiAs-B8 are semi-conductors with energy bandgaps of 0.623, 2.517 and 0.471 eV, while CsCl is metallic with no bandgap. The electron charge density analysis for all ScN phases shows a charge transfer between Sc and N attributing to their electronegativity. The optical properties of ScN phases are investigated. The maximum reflectivity of ScN in CsCl-B2, NaCl-B1, NiAs-B8 and ZB-B3 phases are 0.5 to 0.56 with a photon energy range of 7.5–10 eV. The ScN phases indicate the strongest absorption in the energy range of 0–4 eV. The refractive index for ScN in the energy range of 7.5 to 10 eV phases indicates that the extinction coefficient k is greater than the phase velocity n, showing no light propagation. On the other hand, the phase velocity n is greater than the extinction coefficient k at 0 to 4 eV and 11 to 15 eV energy ranges for all the ScN phases with excellent light propagation, consistent with the conduction curves.

Keywords. Structural stability; DFT calculations; electronic properties; optical properties; transition metal nitrides.

1. Introduction

Scandium nitride (ScN) is one of the transition metal mono-nitrides that possess phenomenal properties, such as mechanical strength, high-temperature stability and high hardness [1]. Moreover, ScN has a high melting point and can be used in high-temperature structural applications or short-wavelength electroluminescent devices [2]. Extensive research based on ScN has been made, specifically on structural, phase transitions and electronic properties [2–10]. A computational study by Takeuchi [3] has been done on the structural and electronic properties of ScN in NaCl-B1, CsCl-B2, NiAs-B8, zinc-blende-B3 and wurtzite-bh structures using the full-potential-linearized augmented plane wave method. It was found that the B1 structure is the ground-state configuration. Similar observation by Meenaatci *et al* [11] was shown when investigating ZrN and HfN in NaCl-B1, CsCl-B2, NiAs-B8, zinc-blende-B3 and wurtzite-bh structures. It was observed that ZrN and HfN are more stable in NaCl-B1. Concentrating on the most thermodynamically stable phase, Duman *et al* [10] have also studied the structure, electronic and dynamical properties of rocksalt ScN compared with III–N semiconductor GaN. Maachou *et al* [5] calculated the electronic properties of scandium III–V compounds ScX (X = N, P, As and Sb) in both B1 and B2 structures and used full-potential-linearized augmented plane wave method to report the transition pressure from the B1-type to B2-type. These calculations indicate that NaCl-B1 phase possesses thermodynamic and mechanical stability at zero pressure. Many studies have been carried out to calculate the structure and electronic properties of ScN in the rocksalt phase, but the optical properties are still very sparse especially for other phases such as CsCl-B2, NiAs-B8 and ZB-B3, respectively. Optical properties constitute the material's response to light and electromagnetic radiation. These properties involve dielectric function, absorbance, reflectance, loss functions and conductivity [12] that can lead to a variety of interesting optical phenomena. Moreover, it will enhance the understanding of specific behaviours of nitrides when affected by light. Therefore, it is worthy to investigate the optical properties of these nitrides. This study aims to investigate the structural, electronic, mechanical and optical properties of ScN in NaCl-B1, CsCl-B2, NiAs-B8 and zinc-blende-B3 phases using first-principle electronic density functional theory. The results obtained here will be compared with existing theoretical and experimental calculations.

Published online: 12 January 2022

2. Computational details

The density functional theory framework [13] is used to calculate the structural, electronic, mechanical and optical properties of ScN nitride in NaCl-B1, CsCl-B2, ZB-B3 and NiAl-B8, using the generalized gradient approximation [14] with Perdew-Burke-Ernzerhof as employed in the CASTEP code [15,16]. To allow the ground-state geometry relaxations, the Broyden–Fletcher–Goldfarb–Shanno algorithms are used to minimize stresses and Hellman-Feynman forces with a maximum force of 0.01 eV $Å^{-1}$. The core and valence interactions are represented by the ultra-soft pseudopotentials [17]. For accurate magnetic moments, we performed geometry optimization where the smearing width was set to 0.001 eV with the displacement of 0.0005 Å and the maximum stress of 0.02 GPa were used for ScN nitride phases, respectively. The plane wave basis was used to represent the wavefunctions of the valence electrons with an energy cutoff of 1000 eV obtained to reach sufficient convergence for all structures of ScN. The Brillouin-zone integrations are performed using the Monkhorst-Pack scheme [18] with a grid size of 18 × 18 × 18 for cubic NaCl-B1, CsCl-B2 and ZB-B3, while for hexagonal NiAl-B8 the grid size was obtained to be 18 x 18 x 10. Both plane-wave energy cutoffs and k-points of ScN structures are used for electronic, mechanical and optical properties. The elastic constants were used to calculate the bulk modulus, shear modulus and Young's modulus. Using the elastic moduli, the Vickers hardness (H_V) was calculated.

The four possible phases of ScN such as: NaCl-B1, CsCl-B2, ZB-B3 and NiAl-B8, have been considered for novel applications whilst, their space groups and atomic positions are listed in table 1. Scandium nitrides (ScN) with the spatial group Fm-3m, Pm-3m, F4-3m and P63/mmc belongs to the cubic and hexagonal crystal structures of NaCl-B1, CsCl-B2, ZB-B3 and NiAs-B8. The fractional coordinates in the NaCl-B1, CsCl-B2, ZB-B3 and NiAs-B8 phases are Sc atoms that occupy positions in corner-site 4a (0, 0, 0) and N atoms that occupy fcc positions 4b (0.5, 0.5, 0.5), (0.5, 0.5, 0.5), (0.25, 0.25, 0.25) and (0.333, 0.667, 0.25) shown in table 1 and figure 1. The electronic configurations of Sc and N atoms are [Ar] $3d^1$ $4s^2$ and [He] $2s^2$ $2p^3$, respectively.

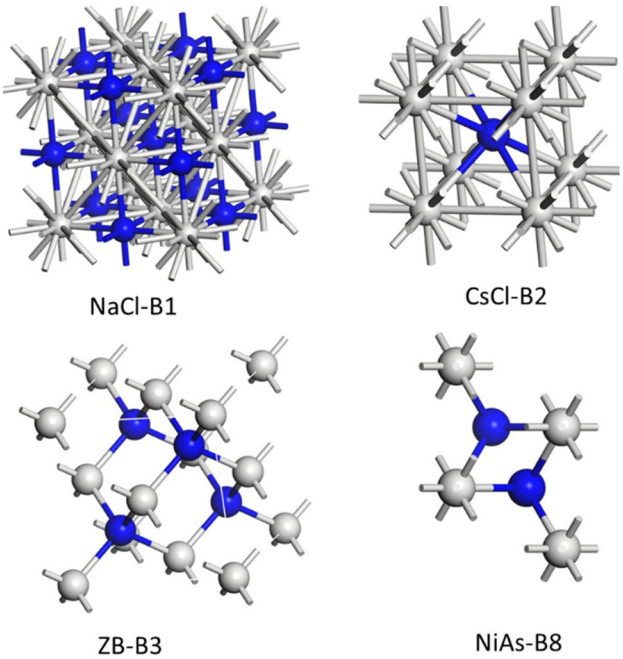

Figure 1. The unit cells of various phases of ScN. The blue colour represents the Scandium atoms, while the grey colour indicates the nitrogen.

3. Results and discussion

3.1 *Structural and mechanical properties*

In table 2, we present the lattice constants (Å), volume ($Å^3$), magnetic moments (μ_B per atom), elastic constants (C_{11}, C_{12}, C_{13}, C_{33} and C_{44}), bulk (B), shear (G) and Young's (E) modulus, a ratio of bulk to shear modulus (B/G), Poisson's ratio (v) for ScN nitride in various NaCl-B1, CsCl-B2, ZB-B3 and NiAs-B8 phases. The calculated lattice constants for NiAl-B1 (4.57 Å), CsCl-B2 (2.82 Å), zinc blende-B3 (4.96 Å) and NiAs-B8 (3.19 Å) agree well with experimental NaCl-B1 (4.50 Å) [19] and calculated NaCl-B1 ScN (4.516, 4.54, 4.55 and 4.57 Å) [3,20,21], CsCl-B2 (2.81 Å), zinc blende-B3 (4.88 Å) and NiAs-B8 (3.10 Å) [3] values, respectively. All the ScN phases are non-magnetic due to zero magnetic moments. In aerospace applications where a

Table 1. Space groups and atomic position of ScN nitride in NaCl-B1, CsCl-B2, zinc-blende-B3 and NiAs-B8 phases.

Phases	Space group	Atomic positions	
		Transition metals	Nitrogen
NaCl-B1	Fm-3m	0, 0, 0	0.5, 0.5, 0.5
CsCl-B2	Pm-3m	0, 0, 0	0.5, 0.5, 0.5
Zinc blende-B3	F4-3m	0, 0, 0	0.25, 0.25, 0.25
NiAs-B8	P63/mmc	0, 0, 0	0.333, 0.667, 0.25

Table 2. Calculated lattice constants (Å), magnetic moments (μ_B per atom), density (g cm^{-3}), elastic constants C_{ij} in GPa, mechanical stability, bulk (B), shear (G) and Young's (E) modulus, the ratio of bulk to shear (B/G), Poisson's ratio (v), Vickers hardness (H_V) and elastic anisotropy (A) of ScN phases such as NaCl-B1, CsCl-B2, zinc-blende-B3 and NiAs-B8.

Structure	NaCl (B1)	CsCl (B2)	Zinc-blende (B3)	NiAs (B8)
a (Å)	4.57	2.82	4.96	3.19
Magnetic moments (μ_B per atom)	0.00	0.00	0.00	0.00
Density (g cm^{-3})	4.12	4.35	3.21	3.98
C_{11}	331.85	571.61	153.87	367.10
C_{12}	96.20	−53.05	107.06	94.73
C_{13}				5.63
C_{33}				521.28
C_{44}	163.85	−101.60	68.84	61.30
C_{66}				136.19
Mechanical stability	S	U	S	S
B (GPa)	174.75	155.17	122.66	162.73
G (GPa)	143.57	−76.13	44.71	112.85
E (GPa)	338.12	205.93	92.85	87.50
B_H/G_H	1.22	−2.04	2.74	1.44
v	0.18	0.79	0.34	0.22
H_V	24.77	–	4.30	17.23
A	0.13	–6.48	1.54	1.60

S, stable; U, unstable.

material's weight is concerned, density plays a significant role and can be calculated with the equation below as

$$\rho^{\text{cal}} = \left(\frac{M_W * N}{\text{Vol} * A_0}\right), \tag{1}$$

where Vol is the volume of the unit cell, M_W is the average molecular weight of the elements in the unit cell, N the total number of atoms and A_0 is the Avogadro's number (6.022 X 10^{23}). The mechanically stable ScN phases such as NaCl-B1, zinc-blende-B3 and NiAs-B8 (4.12, 3.21 and 3.98 g cm^{-3}) possess lower densities than that of $L1_2$ Ni_3Al (6.14 g cm^{-3}) [22] commonly utilized in the aerospace industry. Therefore, these stable ScN phases have the potential to be applied in lightweight applications. We further investigate the elastic properties of a solid specifically, the mechanical behaviour of ScN phases. The elastic properties are calculated in order to explore the mechanical stability of these nitrides. Elastic constants describe the mechanical resistance in a crystal due to applied external stress. In order to determine the total energy variation, a small strain needs to be applied to the unit cell [23,24] and the elastic strain can be calculated as follows:

$$U = \frac{\Delta E}{V_0}\frac{1}{2}\sum_i^6\sum_j^6 C_{ij}e_ie_j, \tag{2}$$

where ΔE is the total energy difference between the deformed and initial unit cell, V_0 is the original cell volume, C_{ij} (i, j = 1 to 6) are the elastic constants and e_i or e_j is the strain. It is well known that cubic and hexagonal structures have three and six independent elastic constants (C_{11}, C_{12}, C_{44} and C_{11}, C_{12}, C_{13}, C_{33}, C_{44}, C_{66}), respectively. While considering the magnetism, the mechanical properties of ScN phases are expected to change. Magnetism can influence the structural stability of a material due to the electron spin magnetic moment [25] and therefore, we included magnetism for all the compounds. However, all the ScN phases are non-magnetic and therefore, the effect of magnetism is not significant. The calculated elastic constants of ScN in NaCl-B1, CsCl-B2, ZB-B3 and NiAs-B8 phases are presented in table 2. The results from this study will be compared with the existing experimental and theoretical data.

For mechanically stable crystals, the elastic constants need to meet the well-known Born-Huang stability criteria [26,27]. The mechanical stability criteria for cubic and hexagonal compounds are as follows:

$$\begin{aligned} &C_{44} > 0;\ C_{11} > C_{12};\ C_{11} + 2C_{12} > 0 \text{ and} \\ &\quad C_{11} > 0, C_{11} - |C_{12}| > 0, \\ &C_{44} > 0,\ (C_{11} + C_{12})C_{33} - 2C_{13}^2 > 0. \end{aligned} \tag{3}$$

In this study, we found only one CsCl phase to be mechanically unstable (denoted as 'U' in table 2) due to not satisfying mechanical stability criteria of equation (3), while others were mechanically stable (indicated with 'S'). Therefore, these mechanically stable ScN compounds can be synthesized experimentally. To further study the mechanical properties of these compounds, the polycrystalline elastic moduli such as shear modulus G, bulk

modulus B and Young's modulus E are investigated. According to the Hill theory [28], the shear modulus of polycrystalline materials can be written as

$$G_H = \frac{G_V + G_R}{2}, \tag{4}$$

where G_v and G_R are Voigt shear modulus and Reuss shear modulus, respectively. G_v and G_R are, respectively, calculated as follows [29–32].

$$G_v = \frac{C_{11} - C_{12} + 3C_{44}}{5} \quad \text{and}$$

$$G_R = \frac{5(C_{11} - C_{12})C_{44}}{4(C_{44} + 3(C_{11} - C_{12})}. \tag{5}$$

For hexagonal compounds, the Voigt and Reuss shear modulus can be expressed as

$$G_V = \frac{1}{30}(7C_{11} - 5C_{12} + 12C_{44} + 2C_{33} - 4C_{13}),$$

$$G_R = \frac{5}{2}\left\{\frac{[(C_{11} + C_{12})C_{33} - 2C_{13}^2]C_{44}C_{66}}{3B_vC_{44}C_{66} + [(C_{11} + C_{12})C_{33} - 2C_{13}^2](C_{44} + C_{66})}\right\} \tag{6}$$

and the VRH mean values are obtained by

$$G_H = \frac{G_V + G_R}{2}. \tag{7}$$

The bulk modulus B and Young's modulus E [33] can be deduced by the following formulae for both cubic and hexagonal compounds. In cubic crystal compounds, B is defined as

$$B = B_H = \frac{B_V + B_R}{2},$$

$$\text{where } B = B_R = B_V = \frac{C_{11} + 2C_{12}}{3} \tag{8}$$

with B_R, $B = B_H$ and B_V being the bulk modulus for Reuss, Voigt and Hill approximations.

For hexagonal structures, B is given by: $B = B_H = \frac{B_V + B_R}{2}$ where B_V and B_R (Voigt and Reuss) bounds are

$$B_V = \frac{2}{9}(C_{11} + C_{12}) + \frac{C_{33}}{2} + 2C_{13} \quad \text{and} \quad B_R = \left(\frac{(C_{11} + C_{12})C_{33} - 2C_{13}^2}{C_{11} + C_{12} + 2C_{33} - 4C_{13}}\right) \tag{9}$$

and Young's modulus is given by

$$E_H = \frac{9B_HG_H}{3B_H + G_H}. \tag{10}$$

Table 2 presents the mechanical properties such as bulk modulus B (GPa), shear modulus G (GPa), Young's modulus E (GPa), a ratio of bulk to shear modulus (B_H/G_H), Poisson's ratio (υ), Vickers hardness (H_V) and elastic anisotropy (A) of ScN phases. The bulk modulus B_H of NaCl-B1 (174.75 GPa) is comparable with the theoretical NaCl-B1 (184.82 GPa) [20] and larger than all the other compounds, while, ZB-B3 (122.66 GPa) is lowest. The slight variance in bulk modulus among the NaCl-B1 ScN vaIues occurs due to the use of different plane wave energy cutoff and the k-points grid. In addition, the bulk modulus B_H can be used as a measure of resistance to volume change by applied pressure [34] and therefore, the calculated bulk modulus B_H shows that NaCl-B1 and ZB-B3 have the strongest and weakest resistance to volume change, respectively. On the other hand, we note that NaCl (143.57 GPa) compared to others has a larger shear moduli G_H, whereas CsCl (–76.13 GPa) has the smaller G_H, indicated in table 2. Shear modulus is closely related to the resistance of the material to plastic deformation [35]. The higher the shear modulus, the stronger is the resistance to reversible deformation on shear stress. Therefore, NaCl-B1 and CsCl-B2 compounds strongly and weakly resist plastic deformation more than other phases. Young's modulus E_H offers a measure of the stiffness of a solid [33], the larger the Young's modulus, the stiffer the material. It is observed that the Young's modulus of NaCl-B1 is larger than other phases and therefore very stiff. Generally, we note that NaCl-B1 has the highest bulk, shear and Young's modulus compared to other ScN phases. In addition, the calculated elastic constants permit us to evaluate some macroscopic properties of the materials such as hardness. In coating application, materials with high hardness measured in Vickers hardness (H_V) are required. The Vickers hardness (H_v) can be evaluated using a theoretical formulation proposed by Tian *et al* [36] as follows:

$$H_V = 0.92K^{1.137}G^{0.708}. \tag{11}$$

The ratio of shear modulus to bulk modulus (G_H/B_H) corresponds to K. The Vickers hardness (H_v) of ScN phases are predicted by using equation (11) and the results are listed in table 2. We note that NaCl-B1 and NiAs are the hardest compounds with the Vickers hardness of 24.77 and 17.23 GPa comparable to the hard material TiN (20.2 GPa) by Shin *et al* [37] and Holleck (21 GPa) [38]. It is common knowledge that the elastic constant C_{44} resists shear distortion with the ability to determine the indentation hardness of a solid indirectly [39–41]. Moreover, shear modulus (G) is the material's ability to oppose shear strain. The hard NaCl-B1 compound possesses not only the higher values of C_{44}, but also larger shear modulus (G) and therefore are resistant to shear deformation. The Pugh's ratio as $K = B_H/G_H$ [34], Cauchy pressure ($P = C_{12}–C_{44}$) [42] and Poisson's ratio (v) = ($3B_H–2G_H$)/($2(3B_H+G_H$) are calculated using the bulk, shear and Young's modulus, shown in table 2, respectively. The conditions are proposed by Pugh [34], Petiffor [42] and Frantsevich *et al* [43], such as $k > 1.75$, $P > 0$ and (v) > 0.25, indicating that the material has a ductile behaviour otherwise it is brittle. From these criteria, we note that zinc blende is ductile compared to NaCl-B1, CsCl-B2 and NiAs-B8, which are brittle. We further calculated the

elastic anisotropy of ScN phases due to its important role in engineering and can be linked to micro-crack induction in materials [44,45]. Anisotropic factor (A) measures the degree of anisotropy in materials and can be evaluated as

$$A = \left(\frac{2C_{44}}{C_{11} - C_{12}}\right). \tag{12}$$

In isotropic crystals, the universal elastic anisotropic index (A) is equal to one. Contrarily, any deviation from one ($A < 1$ or $A > 1$) implies that the material is anisotropic. The calculated universal anisotropic values for ScN phases are indicated in table 2. We note that ScN phases are anisotropic with NiAs phase having the highest anisotropic index of 1.60 and CsCl having the lowest anisotropic index of –6.48.

3.2 *Electronic and magnetic properties*

After performing the geometry optimization, we then calculated the band structures for ScN in NaCl-B1, CsCl-B2, ZB-B3 and NiAs-B8 phases, summarized in figure 2. (Fermi energy level is set to zero for all phases). The calculated band structures suggest that NaCl-B1 (0.623 eV) and NiAs-B8 (0.471 eV) are slightly semi-conductors attributing to their low bandgap almost close to zero. In zinc-blende (ZB) phase, a very large bandgap of 2.517 eV is visible with semi-conducting behaviour, while CsCl-B2 phase indicates a strong overlap in valence–conduction bands around Fermi energy level suggesting a metallic behaviour. These results are in good agreement with previous theoretical data of B1 (0.9 eV) [1,3,20]. Whereas, other experimental and theoretical studies found that ScN has a semimetal behaviour [6]. The subject of ScN being a semi-conductor or semimetal is still a controversy. The electronic partial density of states for ScN in NaCl-B1, CsCl-B2, ZB-B3 and NiAs-B8 phases are shown figure 3. The presence or absence of the d-states around the Fermi energy level (E_f) in a material determines if that material is a conductor, semiconductor or insulator. Since there are no d-states around the Fermi energy (E_f) level in NaCl-B1, ZB-B3 and NiAs-B8, we could see bandgaps with no overlap between the valence and the conduction band around the Fermi energy level in these nitrides.

Therefore, these compounds are semiconductors. Contrarily, no energy bandgap was found in the CsCl-B3 and thus have a metallic behaviour consistent with the band structure analyses and the theoretical study by Takeuchi [3]. Moreover, we can extract the composition in energy bands with the partial density of states. The dominant energy states in the valence region shown in this diagram (figure 3) are those of N—the 2s located at –15 to –10 eV for all the ScN phases, while in the mixed N—the 2p and Sc—4s and 4p energy bands dominates around –5 to 0.5 eV due to the

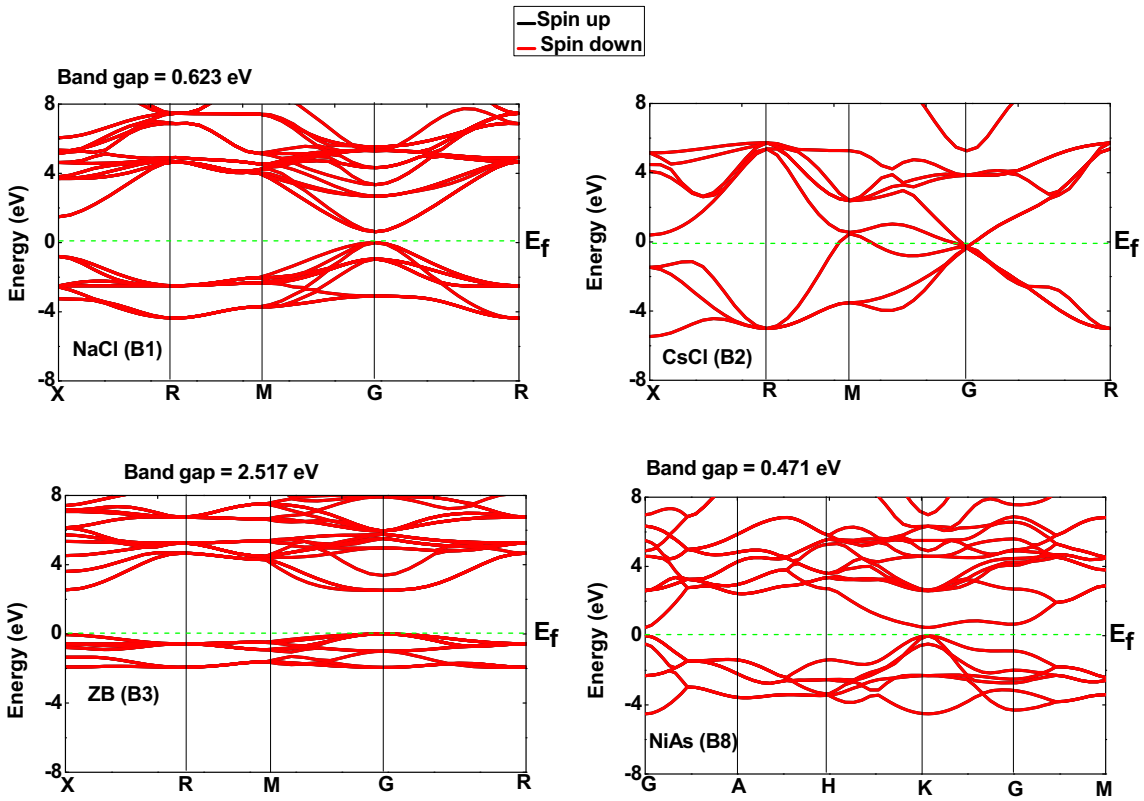

Figure 2. Band structures of the four ScN in NaCl-B1, CsCl-B2, zinc-blende-B3 and NiAs-B8 phases. The Fermi energy level is represented by the dotted line at 0 eV.

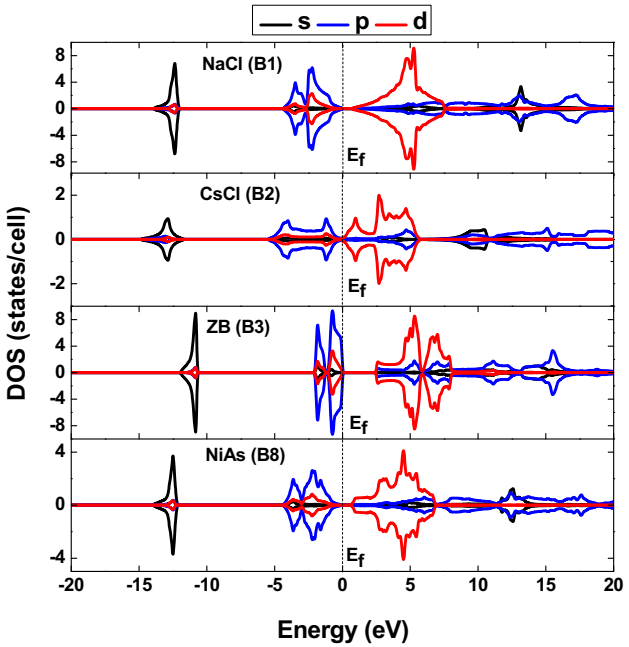

Figure 3. Partial density of states (DOS) of the four ScN in NaCl-B1, CsCl-B2, zinc-blende-B3 and NiAs-B8 phases. The Fermi energy level is represented by the dotted line at 0 eV.

hybridization effects. The d-states of Sc in conduction region dominates from 0 to 8 eV, while the N—2p and Sc—4p states are more predominant from 14 to 20 eV dissipating beyond 20 eV, respectively.

To further investigate the bonding behaviour of ScN in NaCl-B1, CsCl-B2, ZB-B3 and NiAs-B8 phases, electron charge density differences [46,47] are calculated. The electron density difference distribution of ScN phases are shown in figure 4. The electron charge accumulation is represented by the red colour, whereas the blue colour

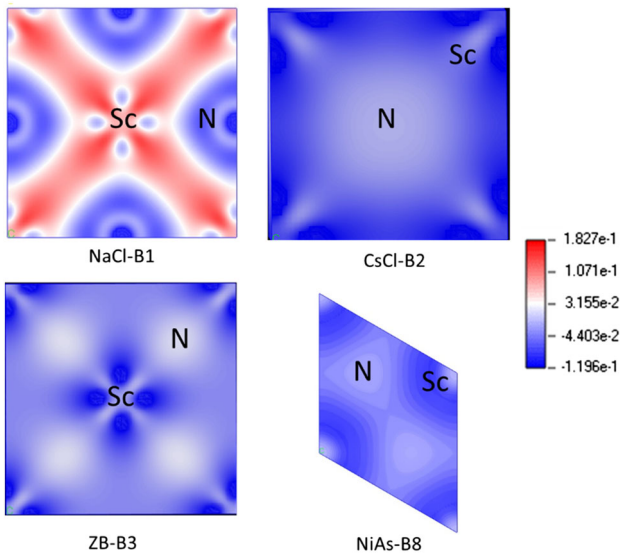

Figure 4. Electron density difference distribution for ScN nitride in NaCl-B1, CsCl-B2, ZB-B3 and NiAs-B8 phases.

shows charge depletion. For comparison, all the ScN phases have the same scale in their density distribution space that surrounds the 3*d*-transition metal and nitrogen ions. From these figures, the charge densities in Nitrogen atoms increases with a decrease in the interstitial Sc atom densities forming metallic bonds (Sc-Sc) for all the phases. These results are consistent with Brik and Ma [20] and Mnisi *et al* [21].

The charge transfer difference in these ScN phases attributes to the difference in electronegativity between the Sc and N atoms, respectively. Therefore, covalent interaction and ionic contribution do exist in these ScN phases, leading to a mixture in bonding such as metallic, covalent and ionic consistent with previous trend [11,20].

3.3 *Optical properties*

The electromagnetic radiation of a material relates to the optical properties such as: dielectric functions, loss functions, reflectance, refractive index, conductivity and absorbance [12], which are calculated in this study. The dielectric function described with an equation: $\varepsilon(\omega) = \varepsilon_1(\omega) + i\varepsilon_2(\omega)$ is an essential parameter that can derive all the other properties mentioned above. The first part of the above equation is the real part $\varepsilon_1(\omega)$ and $i\varepsilon_2(\omega)$ is the imaginary part defined as:

$$i\varepsilon_2(\omega) = \frac{2e^2\pi}{\Omega_{\varepsilon_0}} \sum_{k,v,c} \left| \left\langle \varphi_K^C | \hat{u} * \vec{r} | \right\rangle \varphi_K^V \right|^2 \sigma\left(E_K^C - E_K^V - E\right), \tag{13}$$

where ω is the frequency of light, e the charge of an electron, $\hat{u}$ vector defines the polarization of the incident electric field, φ_K^V and φ_K^C represent the wavefunction at k from valence and conduction bands.

The real part $\varepsilon_1(\omega)$ can be obtained when Kramers-Kronig relation (equation (14)) is applied on the imaginary part of the dielectric function shown below.

$$\varepsilon_1(\omega) = 1 + \frac{2}{\pi} P \int_0^\infty \frac{\omega' \varepsilon_2(\omega')}{\omega'^2 - \omega^2} d\omega', \tag{14}$$

where P is the principal integral value, $\varepsilon_1(\omega)$ and $\varepsilon_2(\omega)$ represent the incident light in equations (13) and (14), respectively. We present the $\varepsilon_1(\omega)$ and $\varepsilon_2(\omega)$ of ScN in NaCl-B1, CsCl-B2, ZB-B3 and NiAs-B8 phases in polycrystalline polarization. The vector directions are taken into a mean isotropic state with no well-defined direction of the incident light. Generally, the electronic properties correlate with the optical properties. The dielectric function property of a material describes the material's response to the incident electromagnetic wave of light. The calculated (a) dielectric function, (b) loss function, (c) reflectivity, (d) refractive index, (e) conductivity and (f) absorbance curves of ScN phases are shown in figure 5, respectively. The graphs with dotted and solid lines represent the imaginary part for the metal conductivity and the real part

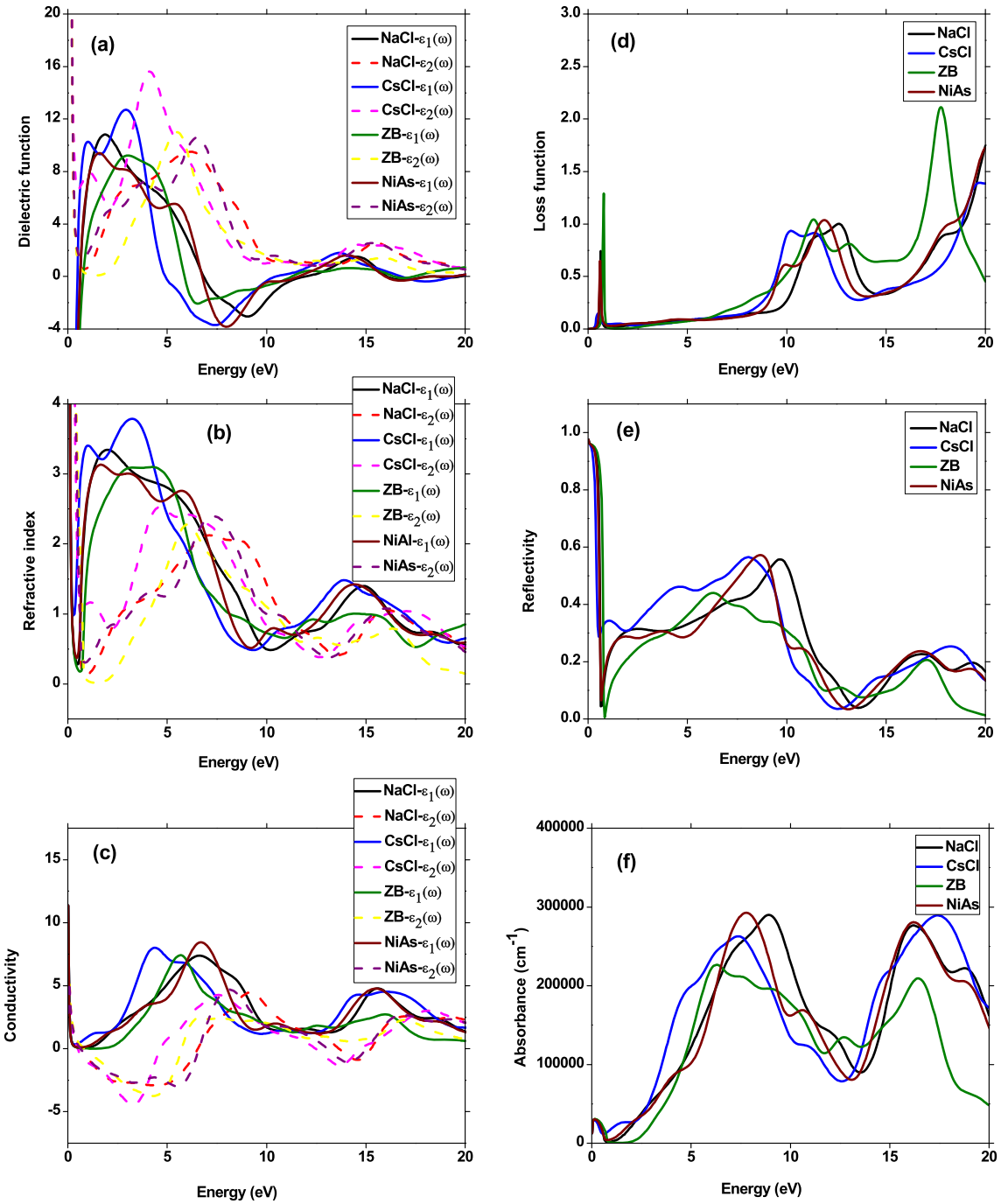

Figure 5. Optical properties of ScN nitride in NaCl-B1, CsCl-B2, ZB-B3 and NiAs-B8 phases such as (**a**) Dielectric function, (**b**) loss function, (**c**) reflectivity, (**d**) refractive index, (**e**) conductivity and (**f**) absorbance respectively. The dotted line indicates imaginary parts whilst the solid line shows the real parts.

indicate the Drude-like behaviour of the dielectric function and conductivity. We set the empirical Drude term with plasma frequency 2 eV and damping 0.04 eV for all ScN in NaCl-B1, CsCl-B2, ZB-B3 and NiAs-B8 phase calculations. We will firstly discuss the imaginary parts $\varepsilon_2(\omega)$ for all the ScN phases and later on will discuss the real part $\varepsilon_1(\omega)$, respectively. The imaginary parts $\varepsilon_2(\omega)$ for ScN in NaCl-B1, ZB-B3 and NiAs-B8 phases starts at 1 eV, except CsCl-B2 starting at 2 eV. The starting energies of NaCl-B1 and NiAs-B8 are larger than their bandgaps of 0.6 and 0.5 eV, CsCl-B2 has no bandgap and ZB-B3 starting energy is smaller than its bandgap of 2.517 eV. In ScN phases $\varepsilon_2(\omega)$ less than 0.5 eV, promotes loss of energy with less absorption. The profiles in $\varepsilon_2(\omega)$ of all the phases have similar trends in the high energy region (0 to 20 eV). The imaginary parts $\varepsilon_2(\omega)$ can be associated with the electron

transition between the valence and conduction bands. There are two highest peaks at 4.0 and 15 eV from CsCl-B2, the peak around 4.5 eV originates from Sc-3d and N-2p in the valence region, while the peak at 15 eV comes from Sc-3d (valence region) and N 2s (conduction region) attributing to electron transition between Sc-3d and N 2p states. For the real part $\varepsilon_1(\omega)$, we observe that the NaCl-B1, CsCl-B2, ZB-B3 and NiAs-B8 phases start at 1 eV with a similar trend in the energy range of 1–20 eV. The CsCl-B2 phase have the highest peaks at 3.0 and 13 eV, the peak around 3.0 eV arises from Sc-3d and N-2p in the valence region, while the peak at 13 eV comes from Sc-3d (valence region) and N 2s (conduction region) due to electron transition between Sc-3d and N 2p states. A number of charge carriers separate dielectric and metallic materials with criteria, such as a larger number of charge carriers corresponds to semi-metallic material, whereas few charge carriers indicate dielectric behaviour. A metallic material can be seen with a negative $\varepsilon_1(\omega)$, while a dielectric material has a positive $\varepsilon_1(\omega)$, respectively. From equation (14), we note that NaCl-B1, CsCl-B2, ZB-B3 and NiAs-B8 phases have metallic behavior at 5-10 eV photon-energies. On the other hand, they indicate semi-conducting (NaCl-B1, ZB-B3 and NiAs-B8) and metallic (CsCl-B2) behaviour from the bandgap analysis. Contrarily, at 1–2.5 eV and 13.5 eV photon-energies, all the ScN possesses a dielectric character. The profile of ScN phases in real parts $\varepsilon_1(\omega)$ possess an analogous trend from 0.5 to 20 eV energy region. We note that in the energy range of 4–11 eV, the $\varepsilon_2(\omega)$ is larger than the $\varepsilon_1(\omega)$ in all phases. Moreover, $\varepsilon_2(\omega)$ is constant at 10–12.5 eV energies indicating absorption characteristics. Refractive index describes the speed of light travelling through a material, where the real part n indicates the phase velocity and the imaginary part k is the extinction coefficient. Figure 5b indicates the refractive index spectra of ScN in NaCl-B1, CsCl-B2, NiAs-B8 and ZB-B3 phases. Notably, the photon energy range of 7.5 to 10 eV in ScN phases indicates the extinction coefficient k greater than the phase velocity n. Therefore, light propagation is prohibited in these energy ranges. On the other hand, the energy range of 0 to 4 eV and 11 to 15 eV shows that the phase velocity n is greater than the extinction coefficient k for all the ScN phases with excellent light propagation. The optical conductivity is a material property, which links the current density to the electric field for general frequencies [48]. Since ScN nitride in CsCl-B2 is metallic with zero bandgap except ScN in NaCl-B1, ZB-B3 and NiAs-B8 phases that are semi-conductors, figure 5c indicates conductivity with zero photon energy for all ScN phases. For the real part, we observed very sharp peaks increasing in ScN phases to reach the maximum values of $\sim$7 to 8.5 with the energy range of 4–7 eV in the ultraviolet region and then decreases to the minimum approaching zero at 16–20 eV energies. We note that in the energy range of 1–6 eV, the $\varepsilon_1(\omega)$ is larger than the $\varepsilon_2(\omega)$ in all phases. Therefore, high conductivity can be expected in that region. These results correspond with the trend observed in the refractive index curve. The energy loss function correlates with the effective Coulomb interaction in a solid and also describes the optical spectra of a material. Figure 5d shows the energy loss spectra of ScN phases in the incident light frequency [49]. The ScN in ZB-B3 have the highest plasma frequency with 17.5 eV energy range at 2.2 loss function. Figure 5e presents the reflectivity spectra for ScN in different phases as a function of photon energy. We note the maximum reflectivity of ScN in CsCl-B2, NaCl-B1 and NiAs-B8 and ZB-B3 at 0.5–0.56 eV nitrides at a photon energy range of (7.5–10 eV). Therefore, a transition from metallic to dielectric response (electric insulator) may arise for all ScN phases if the incident light frequency can be greater than 20 eV [50]. Absorbance defines an ability of a material to absorb energy. Figure 5f shows the absorption spectra for all ScN in NaCl-B1, CsCl-B2, ZB-B3 and NiAs-B8 phases as a function of photon energy. It is noted that the frequency area of 0–2.5 eV is the strongest absorption zone for all ScN phases consistent with the reflectivity and loss function curves at 1 eV. In addition, the NaCl-B1, NiAs-B8 and CsCl-B2 possess the highest absorption peaks around the energy range of 7.5, 9 and 17.5 eV. The equations for absorbance, reflectivity and loss function are omitted here but can be found in the study by Wang *et al* [51], respectively.

4. Conclusion

In conclusion, the ultrasoft pseudopotential method was used to calculate the structural, electronic, mechanical and optical properties of the bulk ScN nitride in NaCl-B1, CsCl-B2, ZB-B3 and NiAl-B8 phases, based on first-principle density functional theory technique. The electronic properties indicate that ScN in NaCl-B1, ZB-B3 and NiAs-B8 are semi-conductors attributing to their visible energy bandgaps, while CsCl-B2 is metallic because of the contributions in metal Sc-d states at the Fermi energy level and the valence–conduction bands overlapping due to hybridization effects. The electron charge distribution plots indicate that there is a charge transfer from nitrogen to the transition metal Sc, respectively. The loss function indicated the highest plasma frequency of ScN in ZB-B3 as 17.5 eV compared to others. Therefore, these results will pave a new understanding of the optical properties in ScN phases for novel applications.

References

[1] Xue W, Yu Y, Zhao Y, Han H and Gao T 2009 *Comput. Mater. Sci.* **45** 1025
[2] Bai X and Kordesch M E 2001 *Appl. Surf. Sci.* **175** 499
[3] Takeuchi N 2002 *Phys. Rev. B* **65** 45204

[4] Uğur S and Soyalp F 2008 *Solid State Commun.* **147** 198
[5] Maachou A, Amrani B and Driz M 2007 *Phys. B Condens. Matter* **388** 384
[6] Travaglini G, Marabelli F, Monnier R, Kaldis E and Wachter P 1986 *Phys. Rev. B* **34** 3876
[7] Stampfl C, Mannstadt W, Asahi R and Freeman A J 2001 *Phys. Rev. B* **63** 155106
[8] Lambrecht W R L 2000 *Phys. Rev. B* **62** 13538
[9] Gu Z, Edgar J H, Pomeroy J, Kuball M and Coffey D W 2004 *J. Mater. Sci. Mater. Electron* **15** 555
[10] Duman S, Bagcı S, Tütüncü H M, Ugur G and Srivastava G P 2006 *Diam. Relat. Mater.* **15** 1175
[11] Meenaatci A T A, Rajeswarapalanichamy R and Iyakutti K 2013 *J. At. Mol. Sci.* **4** 321
[12] Saha S, Sinha T P and Mookerjee A 2000 *Phys. Rev. B-Condens. Matter* **62** 8828
[13] Hohenberg P and Kohn W 1964 *Phys. Rev.* **136** B864
[14] Perdew J, Burke K and Ernzerhof M 1996 *Phys. Rev. Lett.* **77** 3865
[15] Clark S J, Segall M D, Pickard C J, Hasnip P J, Probert M I J, Refson K *et al* 2005 *Zeitschrift Fur Krist.* **220** 567
[16] Segall M D, Lindan P J D, Probert M J, Pickard C J, Hasnip P J, Clark S J *et al* 2002 *J. Phys. Condens. Matter* **14** 2717
[17] Vanderbilt D 1990 *Phys. Rev. B* **41** 7892
[18] Monkhorst H J and Pack J D 1976 *Phys. Rev. B* **13** 5188
[19] Gall D, Petrov I, Hellgren N, Hultman L, Sundgren J E and Greene J E 1998 *J. Appl. Phys.* **84** 6034
[20] Brik M G and Ma C G 2012 *Comput. Mater. Sci.* **51** 380
[21] Mnisi B O, Benecha E M and Tibane M M 2021 *Intermetallics* **137** 107272
[22] Popoola A I and Lowther J E 2014 *Int. J. Mod. Phys. B* **28** 1450066
[23] Heid R, Bohnen K P, Renker B, Wolf T and Schober H 2005 *Phys. Rev. B* **71** 92302
[24] Ding W J, Yi J X, Chen P, Li D L, Peng L M and Tang B Y 2012 *Solid State Sci.* **14** 555
[25] Zhou L, Körmann F, Holec D, Bartosik M, Grabowski B, Neugebauer J *et al* 2014 *Phys. Rev. B* **90** 184102
[26] Born M 1940 *Math. Proc. Cambridge Philos. Soc.* **36** 160
[27] Born M and Huang K 1956 *Theory of crystal lattices* (Oxford: Clarendon Press)
[28] Hill R 1952 *Proc. Phys. Soc. Sect. A* **65** 349
[29] Petrman V and Houska J 2013 *J. Mater. Sci.* **48** 7642
[30] Voigt W 1928 *Lehrbuch der kristallphysik* Teubner Leipzig p 962
[31] Reuss A 1929 *Z. Angew. Math. Mech.* **9** 49
[32] Ganeshan S, Shang S L, Zhang H, Wang Y, Mantina M and Liu Z K 2009 *Intermetallics* **17** 313
[33] McNaught A D 1997 *Compendium of chemical terminology* (Oxford: Blackwell Science)
[34] Pugh S F 1954 *Dublin Philos. Mag. J. Sci.* **45** 823
[35] Hu W C, Liu Y, Li D J, Zeng X Q and Xu C S 2014 *Comput. Mater. Sci.* **83** 27
[36] Tian Y, Xu B and Zhao Z 2012 *Int. J. Refract. Met. Hard Mater.* **33** 93
[37] Shin C S, Gall D, Hellgren N, Patscheider J, Petrov I and Greene J E 2003 *J. Appl. Phys.* **93** 6025
[38] Holleck H 1986 *J. Vac. Sci. Technol. A Vacuum Surfaces Film* **4** 2661
[39] Holec D, Friák M, Neugebauer J and Mayrhofer P H 2012 *Phys. Rev. B* **85** 64101
[40] Liu Z T Y, Burton B P, Khare S V and Gall D 2016 *J. Phys. Condens. Matter* **29** 35401
[41] Zhong Y, Xia X, Shi F, Zhan J, Tu J and Fan H J 2016 *Adv. Sci.* **3** 1500286
[42] Pettifor D G 1992 *Mater. Sci. Technol.* **8** 345
[43] Frantsevich I N, Voronov F F and Bokuta S A 1983 *Elastic constants and elastic moduli of metals and insulators handbook* p 60
[44] Fu H, Li D, Peng F, Gao T and Cheng X 2008 *Comput. Mater. Sci.* **44** 774
[45] Ledbetter H and Migliori A 2006 *J. Appl. Phys.* **100** 63516
[46] Meziane S, Feraoun H, Ouahrani T and Esling C 2013 *J. Alloys Compd.* **581** 731
[47] Li X, Chen D, Wu Y, Wang M, Ma N and Wang H 2017 *AIP Adv.* **7** 065012
[48] Yu G, Lee C H, Heeger A J and Cheong S W 1992 *Physica C Superconductivity* **203** 419
[49] De Almeida J S and Ahuja R 2006 *Phys. Rev. B* **73** 165102
[50] Li X, Cui H and Zhang R 2016 *Sci. Rep.* **6** 1
[51] Wang Q B, Zhou C, Chen L, Wang X C and He K H 2014 *Opt. Commun.* **312** 185